

# Short-range order in GeSn alloy

Boxiao Cao,<sup>†</sup> Shunda Chen,<sup>†</sup> Xiaochen Jin,<sup>†</sup> Jifeng Liu,<sup>‡</sup> and Tianshu Li<sup>\*,†</sup>

<sup>†</sup>*Department of Civil and Environmental Engineering, George Washington University,  
Washington, DC 20052*

<sup>‡</sup>*Thayer School of Engineering, Dartmouth College, Hanover, NH 03755*

E-mail: [tsli@gwu.edu](mailto:tsli@gwu.edu)

## Abstract

Group IV alloys have been long viewed as homogeneous random solid solutions since they were first perceived as Si-compatible, direct-band-gap semiconductors 30 years ago. Such a perception underlies the understanding, interpretation and prediction of alloys' properties. However, as the race to create scalable and tunable device materials enters a composition domain far beyond alloys' equilibrium solubility, a fundamental question emerges as to how random these alloys truly are. Here we show, by combining statistical sampling and large-scale *ab initio* calculations, that GeSn alloy, a promising group IV alloy for mid-infrared technology, exhibits a clear, short-range order for solute atoms within its entire composition range. Such short-range order is further found to substantially affect the electronic properties of GeSn. We demonstrate the proper inclusion of this short-range order through canonical sampling can lead to a significant improvement over previous predictions on alloy's band gaps, by showing an excellent agreement with experiments within the entire studied composition range. Our finding thus not only calls for an important revision of current structural model for group IV alloy, but also suggests short-range order may generically exist in different types of alloys.

# Keywords

Short-range order, GeSn alloy, band gap, Monte Carlo, *ab initio* calculation, random alloy

## 1 Introduction

Since the first prediction in SiGeSn alloy on its direct band gap,<sup>1</sup> group IV alloys have attracted attentions for silicon photonics. This interest has been significantly boosted recently as group IV alloys have been indeed demonstrated viable for optoelectronic applications when a substantial amount of Sn is incorporated into Si and Ge by physical or chemical vapor deposition techniques.<sup>2,3</sup> In particular, with a Sn composition beyond 8 at. %, GeSn alloy was characterized as a direct band gap semiconductor by photoluminescence and lasing.<sup>4-10</sup> As the band gap of GeSn alloy continuously decreases with Sn composition, a high-Sn content GeSn alloy (*e.g.*, >20 at.% Sn) is of particular interest as it enables a wavelength coverage well within the mid-infrared range, thus promising numerous exciting applications including light-emission, chemical and biological sensing.<sup>11</sup>

One of the main challenges in GeSn alloy is Sn segregation, where Sn atoms aggregate in lattice, adversely affecting the properties and integrity of GeSn alloy. To address this issue, experimental characterization has been focused on differentiating Sn segregation from Sn dispersion.<sup>12-15</sup> As a commonly adopted notion, GeSn alloy is viewed as a homogeneous random solid solution when no Sn segregation is present. This assumption has been employed to interpret experiments,<sup>12-17</sup> but more crucially, constitutes the foundation for nearly all theoretical predictions of GeSn alloys.<sup>18-29</sup> Indeed, commonly employed modeling methods, including virtual crystal approximation (VCA), coherent-potential approximation (CPA), and special quasi-random structure (SQS),<sup>30</sup> are all based on this assumption.

Although the absence of Sn cluster certainly indicates atoms are well dispersed within the lattice, it remains unclear whether a well-dispersed Sn distribution necessarily implies a truly random distribution. In a truly random alloy, a lattice site is occupied by constituent

elements with a probability solely depending on alloy's composition, irrespective of what is present in its neighbors. In contrast, in a well-dispersed, but not necessarily truly random alloy, the probability of site occupancy also depends on neighboring atoms, due to a correlation between constituent elements. Both types of distributions lead to a microscopically homogeneous and well-dispersed alloy, *i.e.*, no segregation, but are distinguished by whether a short-range ordering is present.

Indeed, recent experimental studies<sup>31,32</sup> based on extended X-ray absorption fine structure (EXAFS) already showed a lack of Sn-Sn nearest neighbors in GeSn alloy with a Sn content up to 12.4 at. %. Characterization of non-equilibrium SiGeSn ternary alloy by atom probe tomography also showed an unexpected repulsive interaction between Si and Sn.<sup>33</sup> On the other hand, although theory and experiment are found to agree well for low-Sn content GeSn alloy,<sup>17</sup> a significant discrepancy emerges very recently for high-Sn alloys on their fundamental band gaps. In particular, first principle calculations based on a random solution model all suggest GeSn alloys turn into a metal at 25 ~ 28 at. % Sn content,<sup>26-28</sup> whereas very recent optical studies confirm ultra-high-Sn content GeSn alloy still remains as a direct band gap semiconductor,<sup>16,34</sup> for example, a  $E_g^\Gamma=0.15$  eV for a Sn concentration as high as 32 at. %.<sup>16</sup> As recent advance in synthesis enables the growth of high-Sn content alloys far beyond Sn's solubility in Ge and Si,<sup>7,9,10,16,34-36</sup> a fundamental question emerges as to how random these group IV alloys truly are.

Here we examine the fundamental assumption of random solid solution in GeSn alloys by combining statistical sampling based on Monte Carlo method and density functional theory (DFT) calculation. Our study indeed shows that GeSn alloy, in contrast to SiGe alloy and the conventional notion, is clearly not a truly random solid solution, by exhibiting a partial, short-range order (SRO) that becomes particularly prominent in the correlation function involving solute atoms. This SRO is reflected by a lower-than-random solute-solute coordination number in their first coordination shell, and resembles what has been recently observed in metallic alloys.<sup>37-39</sup> Importantly, the identified SRO is further found to

account for the discrepancy between theory and experiment, through our ensemble-averaged prediction that explicitly incorporates the SRO, and shows an excellent agreement with the experiments over the entire composition range studied so far.

## 2 Methods

### 2.1 Metropolis Monte Carlo Sampling

The notion of simple arithmetic average is commonly employed to obtain the average property of interest  $\bar{X}$  in alloy, namely,  $\bar{X} = 1/N \sum_i^N X_i$ , where  $N$  is the number of configurations and  $X_i$  is the property of configuration  $i$ . An underlying assumption for simple average is that all configurations within the ensemble carry the same statistical weight, which is a condition satisfied in truly random solution. In real alloy, each configuration may carry a unique statistical weight  $w_i$ , thus contributing differently to the ensemble average  $\langle X \rangle = \sum_i w_i X_i$ . Under a given temperature  $T$ , such statistical weight is the Boltzmann factor  $w_i = \exp(-E_i/k_B T)/Z$ , where  $E_i$  is the total energy for the configuration  $i$ ,  $k_B$  is the Boltzmann constant, and  $Z$  is the partition function for canonical ensemble. An efficient way of computing the ensemble average  $\langle X \rangle$  is Metropolis Monte Carlo (MC) method,<sup>40</sup> where a new configuration  $j$ , created by a trial move from the current configuration  $i$ , is accepted based on  $w_j/w_i = \exp(-(E_j - E_i)/k_B T)$ . For binary group IV alloy, the trial move involves swapping a randomly selected solute atom with a randomly selected solvent atom within Diamond Cubic (DC) lattice. The new configuration is then fully relaxed by DFT calculation to obtain the total energy  $E$ .

### 2.2 DFT calculations

Our DFT calculation is carried out using the Vienna Ab initio Simulation Package (VASP)<sup>41</sup> based on the projector augmented wave method.<sup>42-44</sup> Local density approximation (LDA)<sup>45</sup> is employed, as previous studies<sup>26,28,29,46</sup> showed LDA yields the best agreement with exper-

iment on pure Ge and Sn for geometry optimization. We also test Perdew-Burke-Ernzerhof (PBE) functional,<sup>47</sup> to ensure the results are robust against the choice of exchange-correlation functionals. Supercells containing 32, 64, and 128 atoms are used to ensure the results are size- and shape independent. A 64-atom supercell is obtained by replicating a conventional DC cell containing 8 atoms twice along each dimension, *i.e.*,  $2 \times 2 \times 2$ , whereas a 32-atom supercell corresponds to a  $2 \times 2 \times 1$  cell. A 128-atom cell is constructed based on the primitive cell of DC structure (containing 2 atoms) by repeating it 4 times along each dimension, *i.e.*,  $4 \times 4 \times 4$ . Because the difference of total energy between two configurations  $\Delta E = E_j - E_i$  is of the central importance for sampling, and  $\Delta E$  converges much faster than  $E$  itself, only Gamma point is used to sample the first Brillouin Zone to enhance computational efficiency. A plane-wave basis with a cutoff energy of 400 eV is used throughout the calculation. For each new configuration, the supercell undergoes full relaxation where both cell geometry and atomic positions are relaxed by conjugate gradient algorithm, with the convergence criteria being  $10^{-4}$  eV and  $10^{-3}$  eV for electronic and ionic relaxations, respectively.

### 2.3 Calculation of radial distribution function

Radial distribution function (RDF) is calculated by randomly choosing 300 ~ 600 snapshots from the obtained MC trajectory based on 64-atom cell, excluding the first 500 configurations due to equilibration. To take thermal motion of atoms into account, *ab initio* molecular dynamics (AIMD) at 300 K is carried out on each configuration for 1 ps, yielding a trajectory of 300 ~ 600 ps from which RDF is calculated. For obtaining RDF of a truly random alloy, a comparable number of configurations are randomly generated, and each undergoes full ionic relaxation, followed by the same AIMD simulation.

### 2.4 Ensemble-averaged band structure calculation

For band structure calculations, we employ the modified Becke-Johnson (mBJ) exchange potential<sup>48</sup> that has been demonstrated to predict the correct band gaps of both Ge and

$\alpha$ -Sn<sup>26,28</sup> with the  $c$ -mBJ parameter set to be 1.2. To recover the Bloch character of electronic eigenstates perturbed by disorder, we apply the spectral weight approach<sup>49,50</sup> through the code *fold2bloch*<sup>50</sup> to unfold the band structures back into the first primitive Brillouin Zone of DC structure. Since the spectral weight approach requires a supercell generated by a translation of primitive cell in real space, band structure calculations are carried out on a 128-atom supercell. To fulfill this requirement, we re-generate the MC trajectory using a 128-atom cell, which, while expensive, also serves as a cross validation of our results against size effect. Spin-orbit coupling (SOC) is also considered in the band structure calculation. Although SOC was demonstrated crucial for reproducing the band structures of Ge and  $\alpha$ -Sn,<sup>26,28</sup> it significantly increases the computational cost, and more importantly, including SOC is found to lead to a rigid shift in direct band gap, virtually independent of configurations (see Supporting Information S2). Therefore, for the part of our study for understanding the role of canonical sampling, we neglect the SOC in the band gap predictions, whereas SOC is included when predicting the concentration dependence of direct band gap.

## 3 Results

### 3.1 Short-range order in solute atoms

Since each atom within a DC lattice is surrounded by four nearest neighbors, the coordination number (CN), which is defined as the number of the nearest neighbors of an atom, is four in elemental semiconductors. If a DC lattice is randomly occupied by element  $A$  and  $B$ , *i.e.*, forming a random solution, then the  $A$ - $A$  or  $B$ - $B$  coordination number is solely determined by the composition of the alloy. For example, a  $\text{Ge}_{0.75}\text{Sn}_{0.25}$  random solution should yield a Sn-Sn CN of one, since one of the four nearest neighbors of each Sn atom, on average, is occupied by a Sn atom, which is set by the overall composition of Sn ( $= 0.25$ ). To examine whether this is true in group IV alloy, we compute the solute-solute coordination number

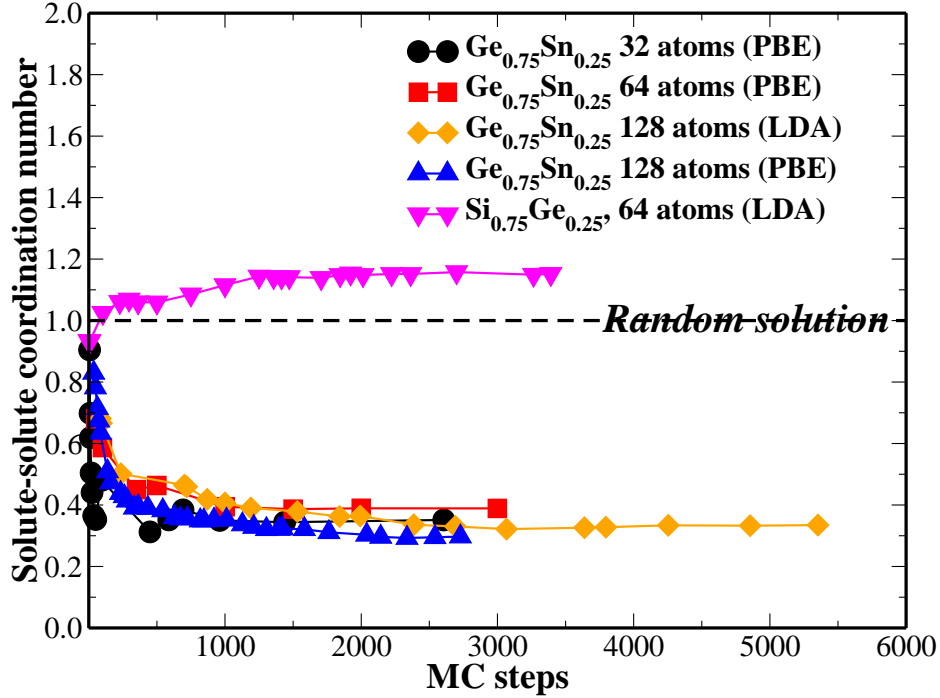


Figure 1: Convergence of the calculated ensemble-averaged solute-solute coordination number in  $\text{Si}_{0.75}\text{Ge}_{0.25}$  and  $\text{Ge}_{0.75}\text{Sn}_{0.25}$  alloys at 300 K, based on the combined MC/DFT method. The dash line indicates the value of solute-solute coordination number in a random solution of the same composition.

in both GeSn (Sn-Sn) and SiGe (Ge-Ge) by integrating the calculated radial distribution function  $g(r)$  based on the obtained MC trajectory.

Fig. 1 shows the variation of the ensemble-averaged solute-solute coordination number with the number of Monte Carlo steps in both  $\text{Ge}_{0.75}\text{Sn}_{0.25}$  and  $\text{Si}_{0.75}\text{Ge}_{0.25}$  alloys at 300 K. It can be seen that beyond  $\sim 1,500$  MC steps, the ensemble-averaged CN has reached a plateau, indicating a numerical convergence. The converged Sn-Sn CNs are further found to be independent of the choice of exchange-correlation functional, or size/shape of the simulation cells, thus confirming the robustness of the results. Interestingly, the ensemble-averaged Ge-Ge coordination number in  $\text{Si}_{0.75}\text{Ge}_{0.25}$  alloy is found to be around 1.1, which is just slightly higher than the ideal value (one) in a truly random  $\text{Si}_{0.75}\text{Ge}_{0.25}$  alloy. This close agreement thus supports the applicability of the random solution model in SiGe alloy, and also confirms the effectiveness of the combined MC/DFT method.

In sharp contrast to SiGe alloy, our calculation shows the ensemble-averaged Sn-Sn coordination number in  $\text{Ge}_{0.75}\text{Sn}_{0.25}$  is only  $0.33 \pm 0.02$  at 300 K, namely, one third of that for a random solution. The significantly lower Sn-Sn coordination number means that there is a depletion of Sn atoms within the first coordination shell of a Sn atom in GeSn alloy, or in other words, there is a strong tendency for a Sn atom to avoid another Sn atom in its first nearest neighbor. Because each Sn atom is four-fold coordinated, the depleted Sn-Sn bonds ( $\sim 2/3$  for each Sn atom) must be compensated by the same number of Sn-Ge bonds. This behavior then clearly indicates that  $\text{Ge}_{0.75}\text{Sn}_{0.25}$  at 300 K deviates from a truly random alloy, *i.e.*, Sn atoms exhibiting some degree of SRO within the alloy. Since the calculated Sn-Sn coordination number is non zero, the identified SRO should be characterized as partial.

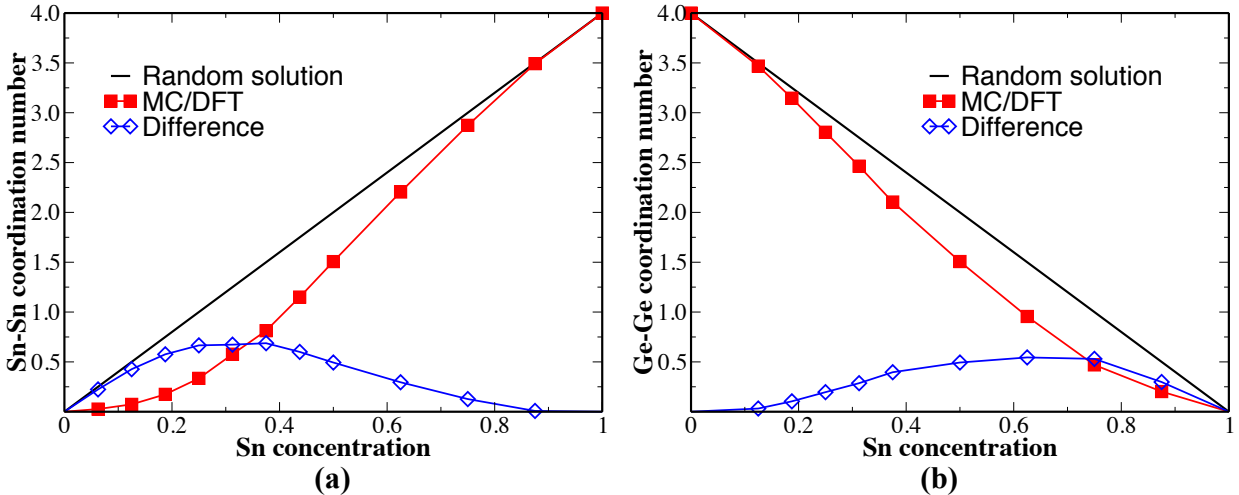


Figure 2: Variation of the ensemble-averaged (a) Sn-Sn coordination number and, (b) Ge-Ge coordination number with Sn concentration in GeSn alloy at 300 K. The error bar of the calculated solute-solute coordination number is about 5 ~ 10% of the mean (see Supporting Information S1 for details), which is about the size of the symbols.

To understand whether such SRO is unique in  $\text{Ge}_{0.75}\text{Sn}_{0.25}$ , or rather generic in all GeSn alloys regardless of its composition, we carry out extensive calculations of Sn-Sn CN within the entire compositional range. As shown in Fig. 2, GeSn alloys of different compositions are all found to exhibit similar behaviors, albeit that the degree of partial ordering varies with composition. In particular, the deviation from the ideal Sn-Sn coordination number is



found to increase quickly with Sn concentration for low-Sn alloy, reach the maximum at a Sn content of around 30 at. %, and then slowly decrease to zero for pure  $\alpha$ -Sn.

Remarkably, we find that the SRO is not just limited to Sn-Sn nearest neighbors, but also exists in Ge-Ge configurations in GeSn alloy. As shown in Fig. 2(b), the calculated Ge-Ge coordination number also displays a deviation from its ideal value, and such deviation is also found to be compositionally dependent. Intriguingly, the composition-dependence in Ge-Ge CN is nearly symmetric to that in Sn-Sn CN: In Ge-rich alloy, the Sn-Sn coordination exhibits a fairly strong SRO while the Ge-Ge distribution stays virtually random; In Sn-rich alloy, the Ge-Ge coordination becomes less random while the Sn-Sn coordination remains nearly random. This contrasting behavior thus indicates that the SRO becomes particularly prominent in the correlation function involving solute or minority atoms in GeSn alloy.

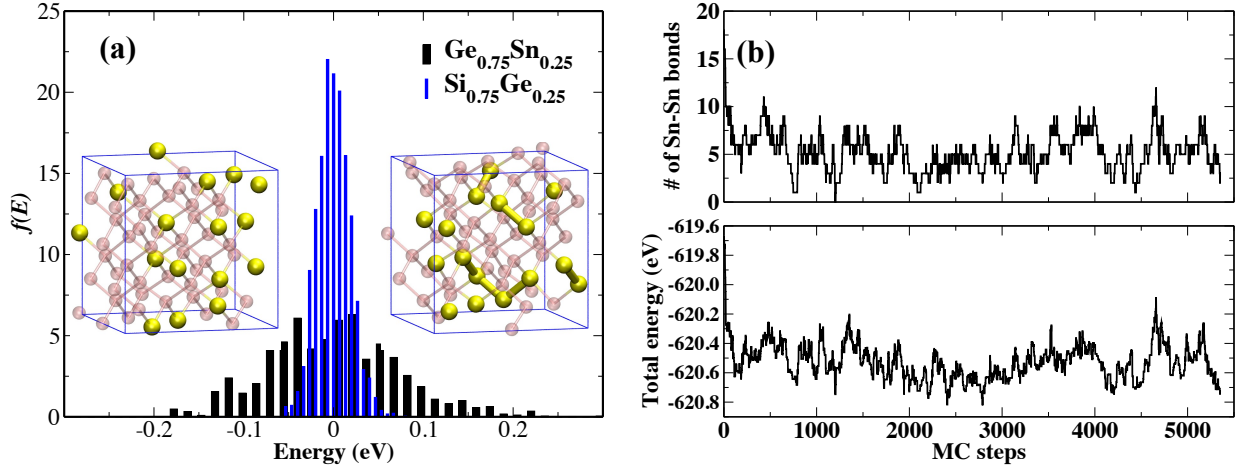


Figure 3: (a) Distribution of total energy  $E$  within the canonical ensembles obtained by MC/DFT calculations for  $\text{Ge}_{0.75}\text{Sn}_{0.25}$  alloy (black) and  $\text{Si}_{0.75}\text{Ge}_{0.25}$  alloy (blue) at 300 K based on a 64-atoms cell. The mean energies  $\langle E \rangle$  for both distributions are set to be zero for the purpose of comparison. Insets show a low-energy configuration on the left and a high-energy configuration on the right. Sn and Ge atoms are represented by yellow and pink spheres, respectively. (b) Variation of the number of Sn-Sn bonds (upper panel) and the total energy (lower panel) in MC trajectory, obtained for  $\text{Ge}_{0.75}\text{Sn}_{0.25}$  at 300 K based on a 128-atom cell.

To understand the origin of this non-random solution behavior in GeSn alloy, we examine the distribution of the total energy  $E$  within the ensemble of configurations, as shown in Fig. 3(a). In  $\text{Ge}_{0.75}\text{Sn}_{0.25}$  alloy, the analysis finds a relatively wide range of distribution of

$E$  for different configurations: from 0.2 eV below to 0.2 eV above the mean energy of the ensemble  $\langle E \rangle$ . As a comparison, the distribution of  $E$  in SiGe alloy is found to be significantly narrower. A wide distribution of  $E$  indicates that a change of atomic configuration in alloy will likely lead to a structure that is energetically very distinct from the original configuration. If the new configuration is strongly unfavorable energetically, it is then less likely to occur within the ensemble, thus having a negligible statistical weight in ensemble average. Toward this end, we examine the structures of  $\text{Ge}_{0.75}\text{Sn}_{0.25}$  alloys located in the different regions of energy distribution, and find that high-energy structures are generally accompanied by a larger number of Sn-Sn pairs, and sometimes even small Sn clusters composed of more than two Sn atoms (see the inset of Fig. 3(a)), whereas in low-energy structures, Sn atoms are largely well dispersed within the Ge matrix, thus avoiding having other Sn atoms as their immediate neighbors. To confirm this observation is of general relevance, we compute the number of Sn-Sn bonds (within a cutoff distance of 3.0 Å) for each configuration within the MC ensemble obtained using 128 atoms for  $\text{Ge}_{0.75}\text{Sn}_{0.25}$  alloy. Fig. 3(b) shows the variation of Sn-Sn bond numbers indeed follows closely the variation of the total energy, suggesting that the nearest neighbor Sn-Sn configurations play a key role in the non-random solution behavior of  $\text{Ge}_{0.75}\text{Sn}_{0.25}$  alloy.

A natural question is then why SRO is prominent in GeSn but not in SiGe alloys, given that both are group IV alloys. A possible explanation can be related to the size difference in group IV elements. As the lattice constants increase slowly from Si (5.43 Å) to Ge (5.66 Å), but rapidly from Ge to  $\alpha$ -Sn (6.46 Å), the lattice mismatch between Ge and  $\alpha$ -Sn (14.1%) is significantly higher than that between Si and Ge (4.2%). Therefore substituting Ge atoms by larger Sn atoms in the DC lattice of Ge will lead to substantial local distortions, which are expected to be higher than those in composition-equivalent SiGe alloys. In particular, such local distortions will become more significant when Sn atoms are located adjacent to each other, which then leads to configurations that are energetically less favorable than those where Sn atoms are well dispersed within the Ge matrix. Indeed, previous theoretical study

showed Sn-Sn interactions are repulsive when Sn atoms serve as substitutional defects in Ge lattice.<sup>51</sup> Similarly, in Sn-rich alloys, substituting Sn atoms in the  $\alpha$ -Sn lattice by smaller Ge atoms will also lead to distortions which become significant if Ge atoms are clustered. This explains why SRO is particularly notable in the solute-solute, rather than solvent-solvent, coordination number in GeSn alloys.

### 3.1.1 Comparison with experiments

Experimental verification of SRO in alloy has been proven challenging, particularly for diffraction-based method, because diffraction contrast arising from local distortion induced by SRO is inherently weak as compared to matrix lattice diffraction.<sup>39</sup> Nevertheless, there exist experimental characterizations on Sn distribution in GeSn alloy, albeit that these characterization studies focused on the subject of Sn segregation or dispersion. Specifically, two types of characterization techniques have been employed: extended X-ray absorption fine structure (EXAFS) which allows probing local environment of atoms, and atom probe tomography (APT) that offers information of atomic positions in 3D. Here we briefly compare our model with experimental results.

EXAFS studies of Sn local environment in GeSn films<sup>31,32</sup> provided the experimental evidence in consistent with the type of SRO in our model. In particular, the fitted Sn-Sn distance based on EXAFS data<sup>31</sup> in GeSn alloy was found to be close to 4 Å, *i.e.*, corresponding to the 2<sup>nd</sup> nearest neighbor (2NN), rather than the 1<sup>st</sup> nearest neighbor (1NN) ( $\sim 2.8$  Å), of Sn in DC lattice. This analysis thus concluded the absence of Sn-Sn dimers or Sn clusters and also indicated the preference of 2NN Sn distribution, which is consistent with the identified SRO in our study where Sn atoms tend to avoid each other in their 1NN. Indeed, as shown in the calculated Sn-Sn radial distribution function (Fig. 4), the first Sn-Sn peak in SRO GeSn is significantly reduced due to a Sn-Sn repulsion, yielding a peak height much lower than that of the second Sn-Sn peak. In contrast, in a truly random GeSn alloy, Sn-Sn peak height decreases with Sn-Sn distance, leading to a peak order opposite to

that of an SRO alloy. We note that this drastic difference in relative peak height can be an important clue for further experimental validation. Interestingly, Ref.<sup>31</sup> concluded GeSn alloys are homogeneous random substitutional alloy, on the basis of a relative increase of Sn atoms in the 2NN of Sn atoms and the absence of Sn cluster. In light of the calculated Sn-Sn RDF, we note that SRO GeSn alloy can be actually indistinguishable from a truly random alloy, if an analysis is carried out only based on 2NN Sn, because as shown in Fig. 4, the second Sn-Sn peak remains virtually unaffected by SRO. In fact, Fig. 4 shows the depletion of Sn atoms within the 1NN is largely compensated by the 3NN, thus leaving 2NN largely intact.

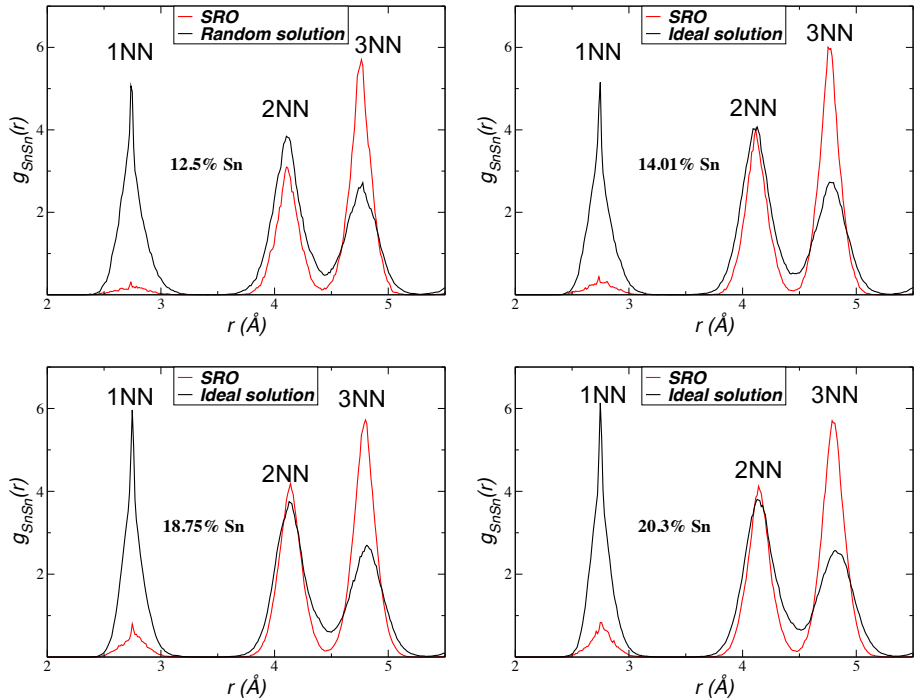


Figure 4: Calculated Sn-Sn radial distribution function of GeSn alloys with SRO (red) and without SRO (black) for different Sn compositions.

On the other hand, a few APT characterization studies<sup>12–14,14,15</sup> were carried out on chemical vapor deposition (CVD) grown GeSn films and nanowires, and showed no Sn segregation or Sn clusters in GeSn alloys. We note that although these studies indicate a well dispersed Sn distribution, the data need to be refined to enable further inferring the occur-

rence of Sn-Sn repulsion in their nearest neighbors. This is because both a SRO-alloy with a low Sn-Sn coordination number and a truly random alloy lead to a well dispersion of Sn atoms, *i.e.*, no Sn segregation, within Ge lattice. In fact, a repulsive Sn-Sn interaction can even facilitate a better Sn dispersion, as there is a lower chance to have a Sn-Sn nearest neighbor in SRO-alloy than in truly random alloy. Therefore a validation of SRO of Sn-Sn repulsion should be obtained by an explicit comparison of Sn-Sn RDF between a truly random model and a SRO model, as suggested in Fig. 4. We also note that a validation of SRO through APT may need a further data processing, analysis, and refinement. For example, the combination of limited detector efficiency and imperfect spatial resolution in APT tends to make data more randomized, as demonstrated in the test of identifying SRO in perfectly ordered compound.<sup>52</sup> In addition, the ablation process of APT in peeling off atoms one-by-one may induce perturbation of atomic positions, which can lead to an artificial atomic distance. Furthermore, as shown in our subsequent study,<sup>53</sup> SRO itself may exhibit a spatial heterogeneity due to strain and composition gradient and a temperature dependence, and depending on the region of samples where APT is performed, SRO may be difficult to probe or even absent. The detailed discussion on validating SRO based on APT will be reported in our subsequent publication.<sup>53</sup>

### 3.2 Effect of SRO on electronic band gaps

An important question is how the identified SRO affects the properties of GeSn alloy, considering nearly all existing theoretical studies<sup>18–26,28,29</sup> were carried out either by simple arithmetic average of randomly generated simulation cells, or by SQS that matches the correlation function of a truly random alloy. To answer this question, we calculate the direct band gap of GeSn alloy, which is a key property for mid-infrared applications. In order to understand the role of SRO, we explicitly compare the ensemble-averaged band gaps  $\langle E_g^\Gamma \rangle$  (canonically sampled) and the simply-averaged band gaps  $\overline{E_g^\Gamma}$  (randomly sampled) of GeSn alloys. The ensemble-averaged band gaps  $\langle E_g^\Gamma \rangle$  are obtained by randomly choosing 50 con-

configurations within the canonical ensemble obtained from MC/DFT trajectory and averaging their respective band gaps, thus reflecting the proper statistical weights of the configurations and by default, taking into account the identified SRO. The validity and effectiveness of this procedure are further confirmed by a convergence test involving 500 configurations (See Supporting Information S3 for more details). In contrast, the simply-averaged band gaps  $\overline{E}_g^\Gamma$  are obtained by randomly generating 50 alloy configurations, from which the band gaps are calculated and averaged. This procedure mimics a completely random solid solution, and indeed reflects the essence underlying the commonly employed theoretical approaches for modeling random alloy, including VCA, CPA and SQS.

Fig. 5(a) shows the comparison of  $\langle E_g^\Gamma \rangle$  and  $\overline{E}_g^\Gamma$  for  $\text{Ge}_{0.875}\text{Sn}_{0.125}$ . It is evident that the ensemble-averaged band gap  $\langle E_g^\Gamma \rangle$  is significantly higher than  $\overline{E}_g^\Gamma$ , by about 100 meV. In addition, the variation of  $E_g^\Gamma$ , as reflected in the error bar of the mean, is also found smaller in  $\langle E_g^\Gamma \rangle$  than in  $\overline{E}_g^\Gamma$ . Such differences clearly demonstrate the quality of alloy structural models, particularly, whether the SRO is taken into account, significantly affects the predicted band gaps of GeSn alloys.

To understand the fundamental origin for this difference, we investigate its correlation with alloys' structures. To this end, it is worth pointing out that a recent study<sup>28</sup> clearly demonstrated the strong influence of Sn configurations on alloy's electronic band gaps. In particular, the study showed the band gap exhibits the maximum when Sn atoms are well separated (without nearest Sn-Sn neighbors), then decreases monotonically as the number of Sn-Sn bonds increases, and reaches the minimum when Sn atoms form a cluster. Motivated by this observation, we examine the general relation between band gaps and alloy structures. As shown in Supporting Information Fig. S4, there indeed exists a general, albeit not perfect, correlation between the number of Sn-Sn bonds and the calculated band gaps: A higher number Sn-Sn bonds overall tends to yield a lower band gap. Since an alloy configuration with a higher number of Sn-Sn bonds is associated with a higher total energy (see Fig. 3(b)), such structure carries a lower statistical weight thus contributes less to the canonical

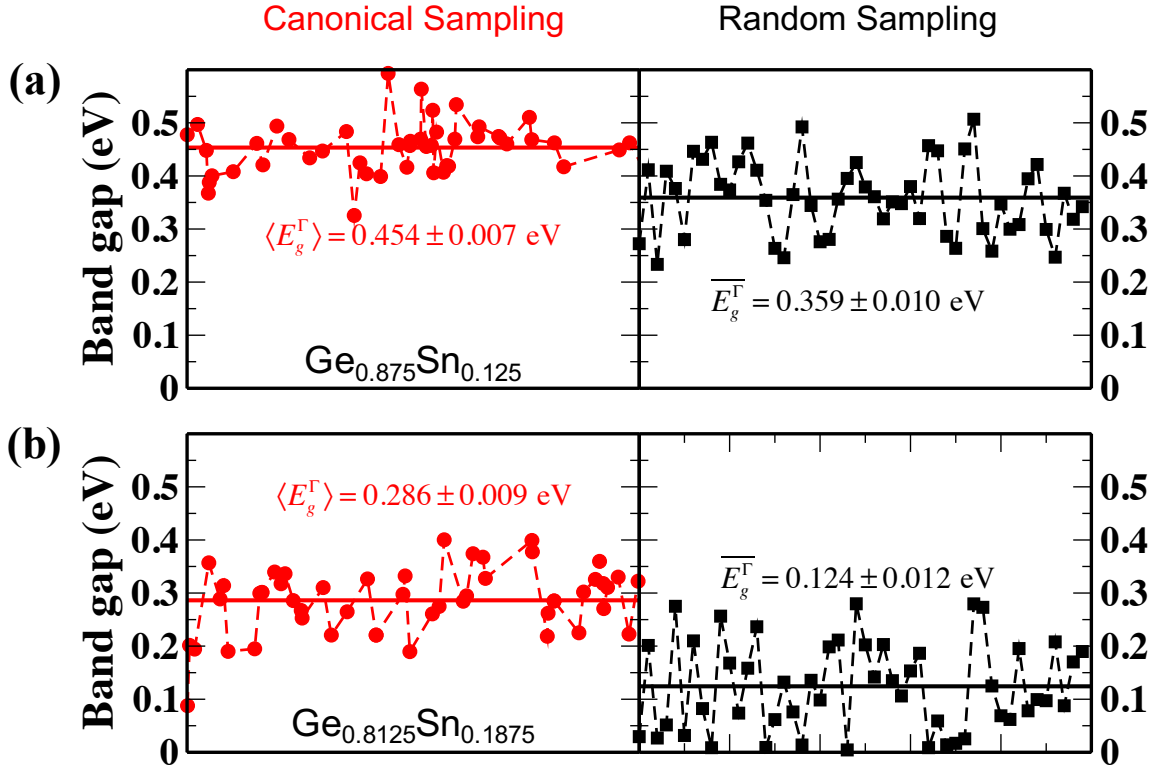


Figure 5: Effect of short-range order on the predicted direct (non-SOC) band gaps of GeSn alloy. The ensemble-averaged band gaps  $\langle E_g^\Gamma \rangle$ , obtained through canonical sampling (left column) are significantly higher than the simply-averaged band gaps  $\overline{E}_g^\Gamma$ , obtained through random sampling (right column), for (a)  $\text{Ge}_{0.875}\text{Sn}_{0.125}$  and (b)  $\text{Ge}_{0.8125}\text{Sn}_{0.1875}$ . The horizontal lines represent the mean gap values.

average. In other words, the SRO plays an important role by limiting the occurrence of those low-gap configurations in the ensemble. This explains why an ensemble-averaged band gap that includes SRO leads to a higher band gap than that inferred from the random solid solution model.

In light of this understanding, and considering that the degree of SRO in Ge-rich GeSn alloy grows with Sn content, as shown in Fig. 2(a), one would expect the correction in the predicted band gaps becomes even more significant for high-Sn content alloy. This is because as Sn content increases, there will be a higher probability of forming Sn-Sn nearest neighbors, or even small Sn clusters, if atoms are randomly distributed within the lattice. To confirm this conjecture, we compare the ensemble-averaged and simply-averaged direct band gap for GeSn alloy containing 18.75 at. % Sn content. As shown by Fig. 5(b), the difference between  $\langle E_g^\Gamma \rangle$  and  $\overline{E}_g^\Gamma$  for  $\text{Ge}_{0.8125}\text{Sn}_{0.1875}$  is indeed found to increase to about 160 meV.

### 3.2.1 Comparison with experiments

To gain a comprehensive understanding on the impact of SRO on the quality of prediction for direct band gap in GeSn alloy, we carry out extensive sampling and calculation to obtain the ensemble-averaged direct band gap as a function of Sn composition. As shown in Fig. 6, our predicted direct band gaps show excellent agreement with experiments<sup>16,34,54</sup> within the entire composition range that has been visited by experiments so far, with the most salient improvements being for those high-Sn content alloys with a Sn content beyond 20 at. %. It is noted that previous studies,<sup>26,28</sup> using the same level of DFT calculation, *i.e.*, mBJ and SOC, but assuming random solid solution, predicted GeSn alloy already becomes a metal at around 25 ~ 28 at. %. Since high-Sn content alloys (with a Sn content beyond 20 at. %) are of particular interest for the proposed mid-infrared applications,<sup>10</sup> our results clearly show that constructing reliable structural models that account for SRO is crucial for predicting and understanding the electronic structures of those alloys.



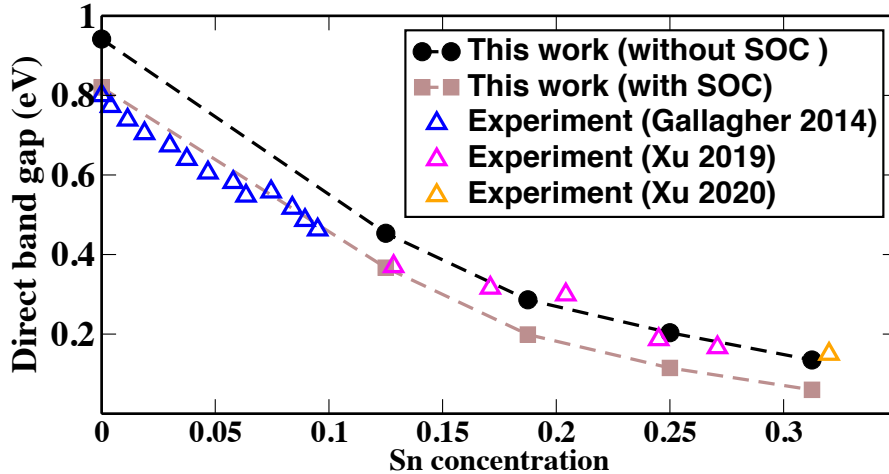


Figure 6: Composition dependence of the direct band gap  $E_g^\Gamma$  in GeSn alloy. The experimentally measured band gaps are from Gallagher 2014,<sup>54</sup> Xu 2019,<sup>34</sup> and Xu 2019.<sup>16</sup>

## 4 Discussion

Our results unravel a subtle but important difference between a homogeneous GeSn alloy with a SRO where Sn atoms tend to avoid each other as their immediate neighbors, and a truly random alloy where a lattice distribution of atoms is completely randomized. Since both types of distributions lead to a well dispersion of Sn atoms in lattice, the absence of Sn segregation cannot be used to infer either scenario. In fact the identified SRO through Sn-Sn repulsion is expected to facilitate a better Sn dispersion, particularly for high-Sn content GeSn alloy. To this end, we note that in addition to the demonstrated corrections to electronic structures, our finding of SRO also has important implications on other properties of GeSn alloys. One such implication is related to understanding the stability of GeSn alloy, as a key challenge in achieving mid-infrared application of GeSn is to ensure alloy is stable enough while incorporating sufficient Sn content (beyond 20 at.%) that is required for covering mid-infrared wavelength. Since these compositions are significantly beyond the

equilibrium solubility of Sn in Ge ( $\sim 1$  at.%) at room temperature, a major expected issue is the segregation of Sn. Interestingly, despite of this concern, high-Sn content GeSn alloys have been recently synthesized through chemical-vapor deposition<sup>16,34,35</sup> and molecular beam epitaxy.<sup>36</sup> Although strain gradient was found to play an important role in incorporating Sn,<sup>35</sup> we conceive that an additional main factor contributing to stability could well be related to the identified lower-than-ideal Sn-Sn coordination number, because a depletion of Sn atoms through a replacement by Ge atoms from their nearest neighbors could greatly reduce the possibility of local gathering of Sn atoms, which is a prerequisite of Sn segregation.

## 5 Conclusion

In summary, by combining Metropolis Monte Carlo sampling and large-scale density functional theory calculations, we reveal the existence of a prominent, non-truly random solution behavior in GeSn alloy within the entire composition range, in contrast to the commonly adopted model of random solution. The calculated solute-solute coordination numbers are found substantially lower than what is assumed by the random solid solution model, demonstrating a partial, short-range order involving solute atoms in GeSn. The identified SRO is consistent with the EXAFS measurement showing a lack of Sn-Sn nearest neighbors in GeSn alloys. When this short-range order is included in modeling through ensemble average, we show the predicted band gaps of GeSn alloys can be significantly improved through an excellent agreement with recent experimental measurements, particularly for high-Sn content GeSn alloys. The identified partial ordering is also expected to play a vital role in understanding the optoelectronic properties and stability of group IV alloys.

## 6 Supporting Information

S1: Estimate of the statistical uncertainty in solute-solute coordination number; S2: Effect of spin-orbit coupling on the predicted direct band gap  $E_g^\Gamma$ ; S3: Convergence of sampling in

computing average band gap  $E_g^\Gamma$ ; S4: Correlation between  $E_g^\Gamma$  and number of Sn-Sn bonds.

## Acknowledgment

The authors thank Prof. Shui-Qing (Fisher) Yu and Dr. Enshi Xu for helpful discussions. This material is based upon work supported by the Air Force Office of Scientific Research under award number FA9550-19-1-0341. The authors acknowledge Department of Defense High Performance Computing Modernization Program for computing support.

## References

- (1) Soref, R. A.; Perry, C. H. Predicted Band Gap of the New Semiconductor SiGeSn. *Journal of Applied Physics* **1991**, *69*, 539–541.
- (2) Gencarelli, F.; Vincent, B.; Demeulemeester, J.; Vantomme, A.; Moussa, A.; Franquet, A.; Kumar, A.; Bender, H.; Meersschaut, J.; Vandervorst, W.; Loo, R.; Caymax, M.; Temst, K.; Heyns, M. Crystalline Properties and Strain Relaxation Mechanism of CVD Grown GeSn. *ECS J. Solid State Sci. Technol.* **2013**, *2*, P134.
- (3) Wirths, S.; Buca, D.; Mantl, S. Si–Ge–Sn Alloys: From Growth to Applications. *Progress in Crystal Growth and Characterization of Materials* **2016**, *62*, 1–39.
- (4) Ghetmiri, S. A.; Du, W.; Margetis, J.; Mosleh, A.; Cousar, L.; Conley, B. R.; Domulevicz, L.; Nazzal, A.; Sun, G.; Soref, R. A.; Tolle, J.; Li, B.; Naseem, H. A.; Yu, S.-Q. Direct-Bandgap GeSn Grown on Silicon with 2230 nm Photoluminescence. *Appl. Phys. Lett.* **2014**, *105*, 151109.
- (5) Wirths, S.; Geiger, R.; von den Driesch, N.; Mussler, G.; Stoica, T.; Mantl, S.; Ikonic, Z.; Luysberg, M.; Chiussi, S.; Hartmann, J. M.; Sigg, H.; Faist, J.; Buca, D.;

- Grützmacher, D. Lasing in Direct-Bandgap GeSn Alloy Grown on Si. *Nature Photonics* **2015**, *9*, 88–92.
- (6) Stange, D.; Wirths, S.; Geiger, R.; Schulte-Braucks, C.; Marzban, B.; von den Driesch, N.; Mussler, G.; Zabel, T.; Stoica, T.; Hartmann, J.-M.; Mantl, S.; Ikonic, Z.; Grützmacher, D.; Sigg, H.; Witzens, J.; Buca, D. Optically Pumped GeSn Microdisk Lasers on Si. *ACS Photonics* **2016**, *3*, 1279–1285.
- (7) Reboud, V.; Gassenq, A.; Pauc, N.; Aubin, J.; Milord, L.; Thai, Q. M.; Bertrand, M.; Guillois, K.; Rouchon, D.; Rothman, J.; Zabel, T.; Armand Pilon, F.; Sigg, H.; Chelnokov, A.; Hartmann, J. M.; Calvo, V. Optically Pumped GeSn Micro-Disks with 16% Sn Lasing at 3.1  $\mu\text{m}$  up to 180 K. *Appl. Phys. Lett.* **2017**, *111*, 092101.
- (8) Al-Kabi, S.; Ghetmiri, S. A.; Margetis, J.; Pham, T.; Zhou, Y.; Dou, W.; Collier, B.; Quinde, R.; Du, W.; Mosleh, A.; Liu, J.; Sun, G.; Soref, R. A.; Tolle, J.; Li, B.; Mortazavi, M.; Naseem, H. A.; Yu, S.-Q. An Optically Pumped 2.5  $\mu\text{m}$  GeSn Laser on Si Operating at 110 K. *Appl. Phys. Lett.* **2016**, *109*, 171105.
- (9) Margetis, J.; Al-Kabi, S.; Du, W.; Dou, W.; Zhou, Y.; Pham, T.; Grant, P.; Ghetmiri, S.; Mosleh, A.; Li, B.; Liu, J.; Sun, G.; Soref, R.; Tolle, J.; Mortazavi, M.; Yu, S.-Q. Si-Based GeSn Lasers with Wavelength Coverage of 2–3  $\mu\text{m}$  and Operating Temperatures up to 180 K. *ACS Photonics* **2018**, *5*, 827–833.
- (10) Dou, W.; Zhou, Y.; Margetis, J.; Ghetmiri, S. A.; Al-Kabi, S.; Du, W.; Liu, J.; Sun, G.; Soref, R. A.; Tolle, J.; Li, B.; Mortazavi, M.; Yu, S.-Q. Optically Pumped Lasing at 3  $\mu\text{m}$  from Compositionally Graded GeSn with Tin up to 22.3%. *Opt. Lett.* **2018**, *43*, 4558–4561.
- (11) Soref, R. Mid-Infrared Photonics in Silicon and Germanium. *Nature Photonics* **2010**, *4*, 495–497.

- (12) Kumar, A.; Komalan, M. P.; Lenka, H.; Kambham, A. K.; Gilbert, M.; Gencarelli, F.; Vincent, B.; Vandervorst, W. Atomic insight into  $\text{Ge}_{1-x}\text{Sn}_x$  using atom probe tomography. *Ultramicroscopy* **2013**, *132*, 171–178.
- (13) Kumar, A.; Demeulemeester, J.; Bogdanowicz, J.; Bran, J.; Melkonyan, D.; Fleischmann, C.; Gencarelli, F.; Shimura, Y.; Wang, W.; Loo, R.; Vandervorst, W. On the interplay between relaxation, defect formation, and atomic Sn distribution in  $\text{Ge}_{(1-x)}\text{Sn}_{(x)}$  unraveled with atom probe tomography. *J Appl Phys* **2015**, *118*, 025302.
- (14) Assali, S.; Dijkstra, A.; Li, A.; Koelling, S.; Verheijen, M. A.; Gagliano, L.; von den Driesch, N.; Buca, D.; Koenraad, P. M.; Haverkort, J. E. M.; Bakkers, E. P. A. M. Growth and Optical Properties of Direct Band Gap  $\text{Ge}/\text{Ge}_{0.87}\text{Sn}_{0.13}$  Core/Shell Nanowire Arrays. *Nano Letters* **2017**, *17*, 1538–1544.
- (15) Assali, S.; Nicolas, J.; Mukherjee, S.; Dijkstra, A.; Moutanabbir, O. Atomically Uniform Sn-Rich GeSn Semiconductors with 3.0–3.5  $\mu\text{m}$  Room-Temperature Optical Emission. *Appl. Phys. Lett.* **2018**, *112*, 251903.
- (16) Xu, C.; Ringwala, D.; Wang, D.; Liu, L.; Poweleit, C. D.; Chang, S. L. Y.; Zhuang, H. L.; Menéndez, J.; Kouvetakis, J. Synthesis and Fundamental Studies of Si-Compatible (Si)GeSn and GeSn Mid-IR Systems with Ultrahigh Sn Contents. *Chem. Mater.* **2019**, *31*, 9831–9842.
- (17) Doherty, J.; Biswas, S.; Galluccio, E.; Broderick, C. A.; Garcia-Gil, A.; Duffy, R.; O’Reilly, E. P.; Holmes, J. D. Progress on Germanium–Tin Nanoscale Alloys. *Chem. Mater.* **2020**, *32*, 4383–4408.
- (18) Shen, J.; Zi, J.; Xie, X.; Jiang, P. Ab Initio Calculation of the Structure of the Random Alloys  $\text{Sn}_x\text{Ge}_{1-x}$ . *Phys. Rev. B* **1997**, *56*, 12084–12087.
- (19) Pandey, R.; Rérat, M.; Causà, M. First-Principles Study of Stability, Band Structure,

- and Optical Properties of the Ordered  $\text{Ge}_{0.50}\text{Sn}_{0.50}$  Alloy. *Appl. Phys. Lett.* **1999**, *75*, 4127–4129.
- (20) Moontragoon, P.; Ikonić, Z.; Harrison, P. Band Structure Calculations of Si–Ge–Sn Alloys: Achieving Direct Band Gap Materials. *Semicond. Sci. Technol.* **2007**, *22*, 742–748.
- (21) Yin, W.-J.; Gong, X.-G.; Wei, S.-H. Origin of the Unusually Large Band-Gap Bowing and the Breakdown of the Band-Edge Distribution Rule in the  $\text{Sn}_x\text{Ge}_{1-x}$  Alloys. *Phys. Rev. B* **2008**, *78*, 161203.
- (22) Beeler, R.; Roucka, R.; Chizmeshya, A. V. G.; Kouvetakis, J.; Menéndez, J. Nonlinear Structure-Composition Relationships in the  $\text{Ge}_{1-y}\text{Sn}_y/\text{Si}(100)$  ( $y < 0.15$ ) System. *Phys. Rev. B* **2011**, *84*, 035204.
- (23) Lu Low, K.; Yang, Y.; Han, G.; Fan, W.; Yeo, Y.-C. Electronic Band Structure and Effective Mass Parameters of  $\text{Ge}_{1-x}\text{Sn}_x$  Alloys. *Journal of Applied Physics* **2012**, *112*, 103715.
- (24) Lee, M.-H.; Liu, P.-L.; Hong, Y.-A.; Chou, Y.-T.; Hong, J.-Y.; Siao, Y.-J. Electronic Band Structures of  $\text{Ge}_{1-x}\text{Sn}_x$  Semiconductors: A First-Principles Density Functional Theory Study. *Journal of Applied Physics* **2013**, *113*, 063517.
- (25) Gupta, S.; Magyari-Köpe, B.; Nishi, Y.; Saraswat, K. C. Achieving Direct Band Gap in Germanium Through Integration of Sn Alloying and External Strain. *Journal of Applied Physics* **2013**, *113*, 073707.
- (26) Eckhardt, C.; Hummer, K.; Kresse, G. Indirect-To-Direct Gap Transition in Strained and Unstrained  $\text{Sn}_x\text{Ge}_{1-x}$  Alloys. *Phys. Rev. B* **2014**, *89*, 165201.
- (27) Freitas, F. L.; Furthmüller, J.; Bechstedt, F.; Marques, M.; Teles, L. K. Influence

- of the Composition Fluctuations and Decomposition on the Tunable Direct Gap and Oscillator Strength of  $\text{Ge}_{1-x}\text{Sn}_x$  Alloys. *Appl. Phys. Lett.* **2016**, *108*, 092101.
- (28) Polak, M. P.; Scharoch, P.; Kudrawiec, R. The Electronic Band Structure of  $\text{Ge}_{1-x}\text{Sn}_x$  in the Full Composition Range: Indirect, Direct, and Inverted Gaps Regimes, Band Offsets, and the Burstein–Moss Effect. *J. Phys. D: Appl. Phys.* **2017**, *50*, 195103.
- (29) O’Halloran, E. J.; Broderick, C. A.; Tanner, D. S. P.; Schulz, S.; O’Reilly, E. P. Comparison of First Principles and Semi-Empirical Models of the Structural and Electronic Properties of  $\text{Ge}_{1-x}\text{Sn}_x$  Alloys. *Opt Quant Electron* **2019**, *51*, 314.
- (30) Zunger, A.; Wei, S.-H.; Ferreira, L. G.; Bernard, J. E. Special Quasirandom Structures. *Phys. Rev. Lett.* **1990**, *65*, 353–356.
- (31) Gencarelli, F.; Grandjean, D.; Shimura, Y.; Vincent, B.; Banerjee, D.; Vantomme, A.; Vandervorst, W.; Loo, R.; Heyns, M.; Temst, K. Extended X-Ray Absorption Fine Structure Investigation of Sn Local Environment in Strained and Relaxed Epitaxial  $\text{Ge}_{1-x}\text{Sn}_x$  Films. *Journal of Applied Physics* **2015**, *117*, 095702.
- (32) Robouch, B. V.; Valeev, R. G.; Kisiel, A.; Marcelli, A. Atomic Distributions Observed in Group IV-IV Binary Tetrahedron Alloys: A Revised Analysis of SiGe and GeSn Compounds. *Journal of Alloys and Compounds* **2020**, *831*, 154743.
- (33) Mukherjee, S.; Kodali, N.; Isheim, D.; Wirths, S.; Hartmann, J. M.; Buca, D.; Seidman, D. N.; Moutanabbir, O. Short-Range Atomic Ordering in Nonequilibrium Silicon-Germanium-Tin Semiconductors. *Phys. Rev. B* **2017**, *95*, 161402.
- (34) Xu, C.; Wallace, P. M.; Ringwala, D. A.; Chang, S. L. Y.; Poweleit, C. D.; Kouvetakis, J.; Menéndez, J. Mid-Infrared (3–8  $\mu\text{m}$ )  $\text{Ge}_{1-y}\text{Sn}_y$  Alloys ( $0.15 < y < 0.30$ ): Synthesis, Structural, and Optical Properties. *Appl. Phys. Lett.* **2019**, *114*, 212104.

- (35) Dou, W.; Benamara, M.; Mosleh, A.; Margetis, J.; Grant, P.; Zhou, Y.; Al-Kabi, S.; Du, W.; Tolle, J.; Li, B.; Mortazavi, M.; Yu, S.-Q. Investigation of GeSn Strain Relaxation and Spontaneous Composition Gradient for Low-Defect and High-Sn Alloy Growth. *Scientific Reports* **2018**, *8*, 5640.
- (36) Imbrenda, D.; Hickey, R.; Carrasco, R. A.; Fernando, N. S.; VanDerslice, J.; Zollner, S.; Kolodzey, J. Infrared Dielectric Response, Index of Refraction, and Absorption of Germanium-Tin Alloys with Tin Contents up to 27% Deposited by Molecular Beam Epitaxy. *Appl. Phys. Lett.* **2018**, *113*, 122104.
- (37) Zhang, F.; Zhao, S.; Jin, K.; Xue, H.; Velisa, G.; Bei, H.; Huang, R.; Ko, J.; Pagan, D.; Neufeind, J.; Weber, W.; Zhang, Y. Local Structure and Short-Range Order in a NiCoCr Solid Solution Alloy. *Phys. Rev. Lett.* **2017**, *118*, 205501.
- (38) Ding, J.; Yu, Q.; Asta, M.; Ritchie, R. O. Tunable Stacking Fault Energies by Tailoring Local Chemical Order in CrCoNi Medium-Entropy Alloys. *PNAS* **2018**, *115*, 8919–8924.
- (39) Zhang, R.; Zhao, S.; Ding, J.; Chong, Y.; Jia, T.; Ophus, C.; Asta, M.; Ritchie, R. O.; Minor, A. M. Short-Range Order and Its Impact on the CrCoNi Medium-Entropy Alloy. *Nature* **2020**, *581*, 283–287.
- (40) Metropolis, N.; Rosenbluth, A. W.; Rosenbluth, M. N.; Teller, A. H.; Teller, E. Equation of State Calculations by Fast Computing Machines. *J. Chem. Phys.* **1953**, *21*, 1087–1092.
- (41) Kresse, G.; Hafner, J. Ab Initio Molecular Dynamics for Liquid Metals. *Phys. Rev. B* **1993**, *47*, 558–561.
- (42) Kresse, G.; Joubert, D. From Ultrasoft Pseudopotentials to the Projector Augmented-Wave Method. *Phys. Rev. B* **1999**, *59*, 1758–1775.



- (43) Kresse, G.; Furthmüller, J. Efficiency of Ab-Initio Total Energy Calculations for Metals and Semiconductors Using a Plane-Wave Basis Set. *Computational Materials Science* **1996**, *6*, 15–50.
- (44) Kresse, G.; Furthmüller, J. Efficient Iterative Schemes for Ab Initio Total-Energy Calculations Using a Plane-Wave Basis Set. *Phys. Rev. B* **1996**, *54*, 11169–11186.
- (45) Ceperley, D. M.; Alder, B. J. Ground State of the Electron Gas by a Stochastic Method. *Phys. Rev. Lett.* **1980**, *45*, 566–569.
- (46) Haas, P.; Tran, F.; Blaha, P. Calculation of the Lattice Constant of Solids with Semilocal Functionals. *Phys. Rev. B* **2009**, *79*, 085104.
- (47) Perdew, J. P.; Burke, K.; Ernzerhof, M. Generalized Gradient Approximation Made Simple. *Phys. Rev. Lett.* **1996**, *77*, 3865–3868.
- (48) Tran, F.; Blaha, P. Accurate Band Gaps of Semiconductors and Insulators with a Semilocal Exchange-Correlation Potential. *Phys. Rev. Lett.* **2009**, *102*, 226401.
- (49) Popescu, V.; Zunger, A. Effective Band Structure of Random Alloys. *Phys. Rev. Lett.* **2010**, *104*, 236403.
- (50) Rubel, O.; Bokhanchuk, A.; Ahmed, S. J.; Assmann, E. Unfolding the Band Structure of Disordered Solids: From Bound States to High-Mobility Kane Fermions. *Phys. Rev. B* **2014**, *90*, 115202.
- (51) Fuhr, J. D.; Ventura, C. I.; Barrio, R. A. Formation of Non-Substitutional  $\beta$ -Sn Defects in  $\text{Ge}_{1-x}\text{Sn}_x$  Alloys. *Journal of Applied Physics* **2013**, *114*, 193508.
- (52) Marceau, R. K. W.; Ceguerra, A. V.; Breen, A. J.; Raabe, D.; Ringer, S. P. Quantitative chemical-structure evaluation using atom probe tomography: Short-range order analysis of Fe–Al. *Ultramicroscopy* **2015**, *157*, 12–20.

(53) To be submitted for publication.

(54) Gallagher, J. D.; Senaratne, C. L.; Kouvetakis, J.; Menéndez, J. Compositional Dependence of the Bowing Parameter for the Direct and Indirect Band Gaps in  $\text{Ge}_{1-y}\text{Sn}_y$  Alloys. *Appl. Phys. Lett.* **2014**, *105*, 142102.